Human Molecular Genetics, 2019, Vol. 28, No. 8 1286–1297

doi: 10.1093/hmg/ddy431
Advance Access Publication Date: 17 December 2018
General Article

GENERAL ARTICLE

FOXF2 is required for cochlear development in humans and mice

Guney Bademci[1], Clemer Abad[1], Armagan Incesulu[2], Fahed Elian[3], Azadeh Reyahi[4], Oscar Diaz-Horta[1], Filiz B. Cengiz[1], Claire J. Sineni[1], Serhat Seyhan[1,5], Emine Ikbal Atli[6], Hikmet Basmak[7], Selma Demir[6], Ali Moussavi Nik[4], Tim Footz[3], Shengru Guo[1], Duygu Duman[8], Suat Fitoz[9], Hakan Gurkan[6], Susan H. Blanton[1,10,11], Michael A. Walter[3], Peter Carlsson[4], Katherina Walz[1,11,12] and Mustafa Tekin[1,10,11,*]

[1]John P. Hussman Institute for Human Genomics, University of Miami Miller School of Medicine, Miami, FL 33136, USA, [2]Department of Otolaryngology—Head and Neck Surgery, Eskisehir Osmangazi University, 26040 Eskisehir, Turkey, [3]Department of Medical Genetics, Faculty of Medicine and Dentistry, University of Alberta, Edmonton, AB T6G 2R3, Canada, [4]Department of Chemistry and Molecular Biology, University of Gothenburg, PO Box 462, SE-405 30 Gothenburg, Sweden, [5]Department of Medical Genetics, Bakirkoy Dr Sadi Konuk Research and Training Hospital, 34147 Istanbul, Turkey, [6]Department of Medical Genetics, Faculty of Medicine, Trakya University, 22030 Edirne, Turkey, [7]Department of Ophthalmology, Eskisehir Osmangazi University, 26040 Eskisehir, Turkey, [8]Division of Pediatric Genetics, Ankara University School of Medicine, 06100 Ankara, Turkey, [9]Department of Radiology, Ankara University School of Medicine, 06100 Ankara, Turkey, [10]Department of Otolaryngology, University of Miami Miller School of Medicine, Miami, FL 33136, USA, [11]Dr John T. Macdonald Foundation Department of Human Genetics, University of Miami Miller School of Medicine, Miami, FL 33136, USA and [12]Department of Medicine, University of Miami Miller School of Medicine, Miami, FL 33136, USA

*To whom correspondence should be addressed at: Dr. John T. Macdonald Department of Human Genetics, Miller School of Medicine, University of Miami, 1501 NW 10th Avenue, BRB-610 (M-860), Miami, FL 33136, USA. Tel: +305 2432381; Fax: +305 2432704; Email: mtekin@med.miami.edu

Abstract

Molecular mechanisms governing the development of the human cochlea remain largely unknown. Through genome sequencing, we identified a homozygous *FOXF2* variant c.325A>T (p.I109F) in a child with profound sensorineural hearing loss (SNHL) associated with incomplete partition type I anomaly of the cochlea. This variant is not found in public databases or in over 1000 ethnicity-matched control individuals. I109 is a highly conserved residue in the forkhead box (Fox) domain of FOXF2, a member of the Fox protein family of transcription factors that regulate the expression of genes involved in embryogenic development as well as adult life. Our *in vitro* studies show that the half-life of mutant FOXF2 is reduced compared to that of wild type. *Foxf2* is expressed in the cochlea of developing and adult mice. The mouse knockout of *Foxf2*

Received: September 24, 2018. **Revised:** December 10, 2018. **Accepted:** December 12, 2018

shows shortened and malformed cochleae, in addition to altered shape of hair cells with innervation and planar cell polarity defects. Expressions of *Eya1* and *Pax3*, genes essential for cochlear development, are reduced in the cochleae of *Foxf2* knockout mice. We conclude that FOXF2 plays a major role in cochlear development and its dysfunction leads to SNHL and developmental anomalies of the cochlea in humans and mice.

Introduction

Sensorineural hearing loss (SNHL) is diagnosed in 1 to 2 per 1000 newborns (1). In ~20% of individuals with congenital SNHL, embryonic development of the inner ear is disturbed, leading to inner ear anomalies (1,2). Anomalies of the inner ear can be diagnosed by imaging studies and often include malformations of the cochlea, the human hearing organ (3,4). While many genes involved in cochlear development have been reported in mice, mutations in very few have been shown to cause cochlear malformations in humans; thus, their roles in human cochlear development remain unknown. Well-recognized genes implicated in cochlear malformations in humans with similar phenotypes in mice include *CHD7* (MIM 608892), *EYA1* (MIM 601653), *FGF3* (MIM 164950), *PAX3* (MIM 606597), *ROR1* (MIM 602336), *SLC26A4* (MIM 605646) and *SOX10* (MIM 602229) (5–9). However, most individuals with cochlear malformations do not have mutations in any of these genes. Therefore, there is a crucial need to identify the underlying genetic mutations in these people and to characterize the roles of affected genes in cochlear development via animal models.

The inner ear has a complex architecture that consists of a collection of different cell types. The vertebrate inner ear develops from the otic placode, which requires highly orchestrated processes to establish otic identity in early development including modeling the structure with morphogenetic movements, expression of cell specific proteins and differentiation of the highly specialized cell types (5,10). Numerous pathways and genes are involved in these processes, such as fibroblast growth factors (FGFs), bone morphogenetic proteins (BMPs), Hedgehog signaling, Wnt signaling and forkhead box (Fox) proteins (5–9).

Fox transcription factors regulate diverse biological processes throughout development and adult life (11). There are currently more than 50 recognized Fox genes in humans and mice (12). In mammals, Fox transcription factors are categorized into subclasses A to S based on sequence similarity (13,14). While all Fox transcription factors share a distinctive DNA-binding Fox domain with differing DNA-binding specificity (15), the divergent sequences outside of the conserved DNA-binding domain likely differentiate the function of these proteins in conjunction with distinct temporal and spatial gene activation patterns (12). In many cases, the absence of even a single Fox transcription factor is lethal. Mutations in some Fox genes are associated with human disease. For example, germline mutations in *FOXC1* (MIM 601090), *FOXL2* (MIM 605597), *FOXP2* (MIM 605317) and *FOXP3* (MIM 300292) cause anterior segment dysgenesis 3 of the eye (MIM 601631), blepharophimosis–ptosis–epicanthus inversus syndrome (MIM 110100), speech-language disorder 1 (MIM 602081) and X-linked immunodysregulation–polyendocrinopathy–enteropathy syndrome (MIM 304790), respectively (16–19). Recently, an autosomal recessive form of SNHL associated with distal renal tubular acidosis has been reported to be caused by *FOXI1* mutations (20).

In this study, we report a homozygous mutation in *FOXF2* (MIM 603250), the underlying cause of a cochlear malformation and SNHL. Further characterization of Foxf2 in mice reveals that it is a fundamental protein for proper cochlear development.

Results

The proband is a child with non-syndromic deafness and incomplete partition type I cochlear malformation

The proband, a 10-year-old girl, was born to first-cousin parents with normal hearing; they also have a hearing daughter (Fig. 1A). She was diagnosed with congenital profound SNHL (Fig. 1B). Audiograms of both parents and the unaffected sister are normal, except that the father has noise-induced hearing loss due to noise exposure in his work environment. Development of gross motor skills is normal, and a clinical examination shows normal tandem walking with a negative Romberg's test. A high-resolution temporal bone computerized tomography of the proband shows bilateral cochleae lacking the entire modioli and cribriform areas, resulting in a cystic appearance, which is consistent with incomplete partition type I anomaly (cystic cochleovestibular malformation; Fig. 1C). An ophthalmological examination shows bilateral hypermetropia and retinal folding without anterior segment anomalies, glaucoma or other retinal abnormalities. A thorough clinical evaluation does not show any other anomalies in the proband, especially no cleft lip or palate or gastrointestinal abnormalities.

Exome and genome sequencing reveal the *FOXF2* p.I109F variant

Initially, DNA samples of the proband and both parents underwent whole exome sequencing (WES). The coverage of targeted exome regions (DNA regions captured by Agilent SureSelect Human All Exon V6) for 10-fold read depth was 87%, 85% and 86% while the average read depth was 55×, 48× and 52× for the father, mother and proband, respectively.

After discovering a candidate DNA variant, DNA samples of the proband, unaffected sister and both parents underwent whole genome sequencing for a more comprehensive analysis. On average, read depth was 44×; 99.31% of the genome was covered by at least 1×, 99.02% by at least 4× and 98.27% by at least 10× coverage (Supplementary Material, Table S1).

We first evaluated the proband's exome and genome for variants in recognized genes for SNHL retrieved from the Hereditary Hearing Loss Homepage (http://hereditaryhearingloss.org/) and Online Mendelian Inheritance in Man (http://omim.org/). This analysis did not reveal a plausible variant under any inheritance model. We subsequently evaluated the variants in the family, which mapped to runs of homozygosity (Supplementary Material, Tables S2 and S3) in the proband, had an allele frequency of <0.005 in gnomAD (global allele frequency) and a read depth of ≥10. From this list, we only kept those variants for which the unaffected sister was not homozygous. Four candidate variants in *FOXF2*, *RREB1*, *AFAP1L2* and *PRB2* remained (Supplementary Material, Table S4). After applying a conservation filter (The Genomic Evolutionary Rate Profiling (GERP) score of >2), *in silico* prediction tools (MutationAssessor, SIFT, MutationTaster, FATHMM and PROVEAN), Combined Annotation-Dependent Depletion (CADD) and Deep Annotation-Dependent Neural Network (DANN) score filters, a single variant remained:

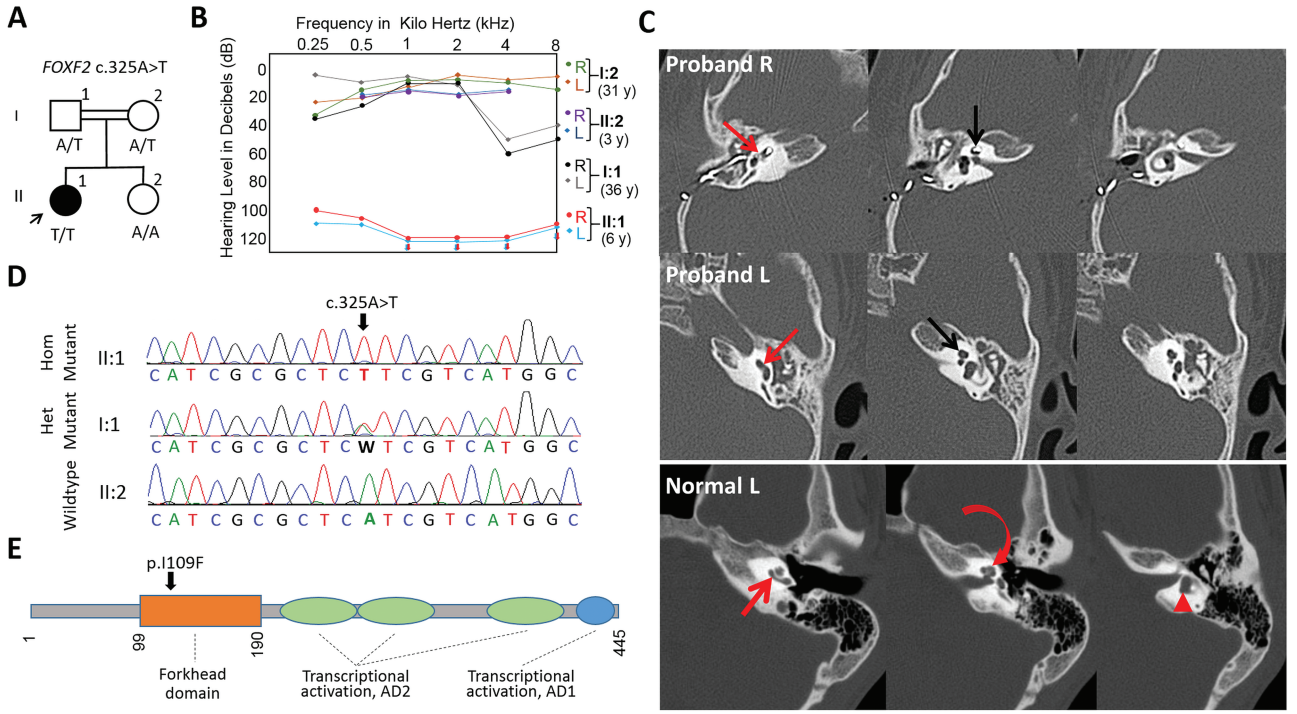

Figure 1. Phenotype and genetic studies of the family. (**A**) Pedigree of the family and segregation of the variant. (**B**) Hearing thresholds of the proband and family members: R, right; L, left. (**C**) Computerized tomography showing incomplete partition type I anomaly bilaterally (upper row, right ear; middle row, left ear). Cochlea is dysplastic. A structure compatible with basilar turn (red arrow) is visible but cochlear apex is cystic (black arrow). There is a cochlear implant on the right side. Please note the bilateral soft tissue in the middle ear cavity (otitis media). Lower row belongs to a normal computerized tomography image of left temporal bone. Normal cochlea with basal turn (red arrow) and apex (curved arrow) along with the vestibule (arrowhead) is shown. (**D**) Electropherogram of the *FOXF2* c.325A>T (p.I109F) variant. Hom, homozygous; Het, heterozygous. (**E**) Localization of the p.I109F variant in FOXF2.

NM_001452.1:c.325A>T (p.I109F) in *FOXF2* (Supplementary Material, Table S4. All autozygous regions were fully covered with genome sequencing (Supplementary Material, Table S3).

Sanger sequencing confirmed that the proband was homozygous and both parents were heterozygous for the variant. The unaffected sister was homozygous for the wild-type (WT) allele (Fig. 1A and D). The DNA position affected by the variant is highly conserved (GERP: 3.99). The variant is not found in dbSNP, EVS or gnomAD population databases, and multiple lines of *in silico* analysis predict it as damaging, high impact or disease causing (Supplementary Material, Tables S4 and S5). We did not see the p.I109F variant in 1042 Turkish control individuals. The variant is located in the Fox domain of FOXF2 (Fig. 1E). I109 is highly conserved in both orthologs and paralogs (Fig. 2A). It has been shown that variants affecting the same amino acid residue of a Fox domain in other Fox family genes cause anterior segment dysgenesis 3 (*FOXC1*; p.I87M), blepharophimosis–ptosis–epicanthus inversus syndrome (*FOXL2*; p.I63T) and X-linked immunodysregulation–polyendocrinopathy–enteropathy syndrome (*FOXP3*; p.I346T; Fig. 2A) (21–24).

FOXF2 p.I109F is less stable than WT FOXF2

To understand the effect of the p.I109F variant in the subcellular localization of FOXF2, we overexpressed the WT and mutant genes in COS-7 cells. These studies show that both FOXF2 forms localize to the nucleus (Supplementary Material, Fig. S1).

To assess the stability of FOXF2, FOXF2 (WT)- and FOXF2 (I109F)-transfected HeLa cells were treated with cycloheximide (50 µg/ml). Immunoblotting experiments were then performed in the supernatant of the cell lysate following centrifugation to measure FOXF2 protein levels after cycloheximide treatment. These experiments show that the I109F mutation causes the mutant FOXF2 to have a shorter half-life than the WT FOXF2. Therefore, the stability of the mutant FOXF2 protein in the proband is expected to be substantially reduced (Fig. 2B). While not likely, an alternative explanation for the loss of FOXF2 in the supernatant fraction may also be due in part, or perhaps entirely, to the mutant FOXF2 protein being in the pelleted fraction discarded.

Expression and role of *Foxf2* in mouse inner ear

We evaluated *Foxf2* expression in a variety of mouse tissues, including the cochlea and the inner ear. Total RNA was isolated from WT mice at E17.5, P0 and P15. Reverse transcription polymerase chain reaction (RT-PCR) with a forward primer located in exon 1 and a reverse primer in exon 2 of the gene produced a unique band of 201 bp corresponding to the WT mRNA. Consistent with previous reports (25), the amplification product was present in cDNA from all analyzed tissues derived from WT mice, notably the inner ear, with the exception of the kidney and the liver. In addition, we found that *Foxf2* is expressed in the inner ear, specifically in the cochlea, in E17.5, P0 and P15 (Supplementary Material, Fig. S2). Reported expression for *Foxf2* within the gEAR—gene Expression Analysis Resource web portal (https://umgear.org/)—and the Shared Harvard Inner-Ear Laboratory Database (https://shield.hms.harvard.edu/about_us.html) is in accordance with our findings, demonstrating that *Foxf2* is expressed in the inner hair cells (IHCs), outer hair cells (OHCs) and supporting cells during development and postnatally (Supplementary Material, Table S6).

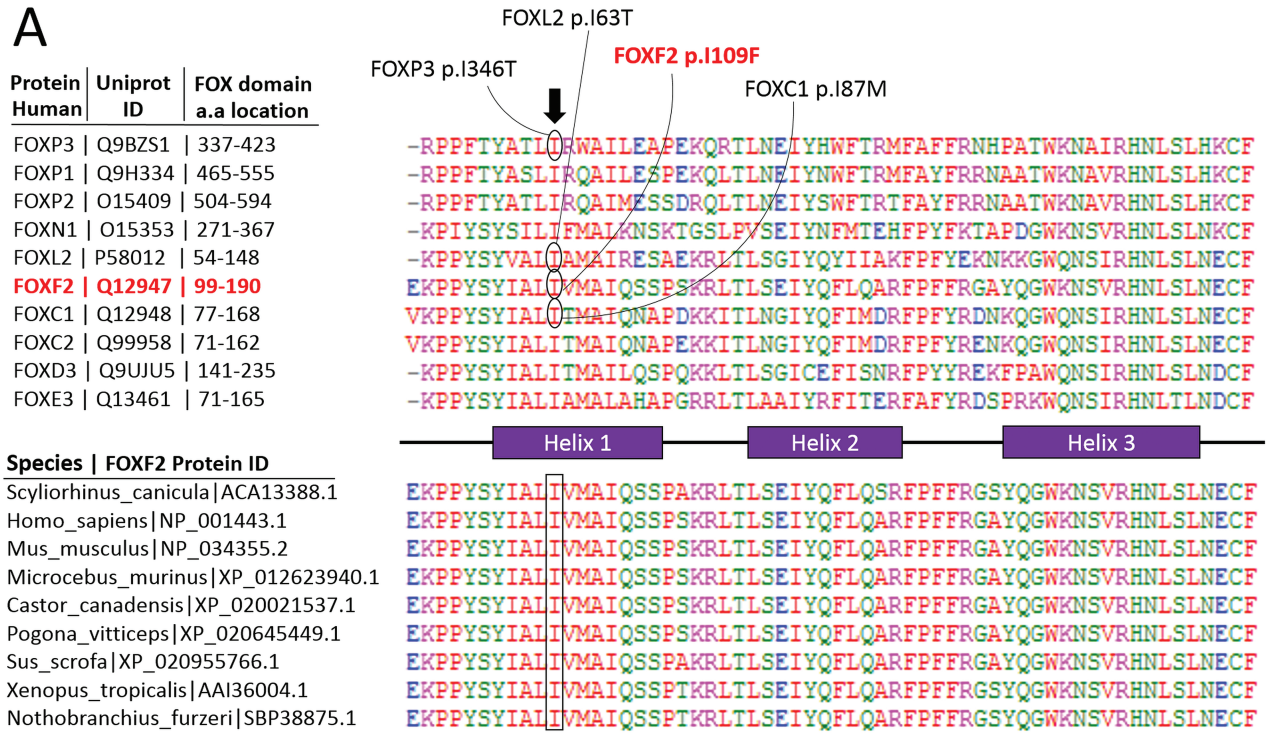

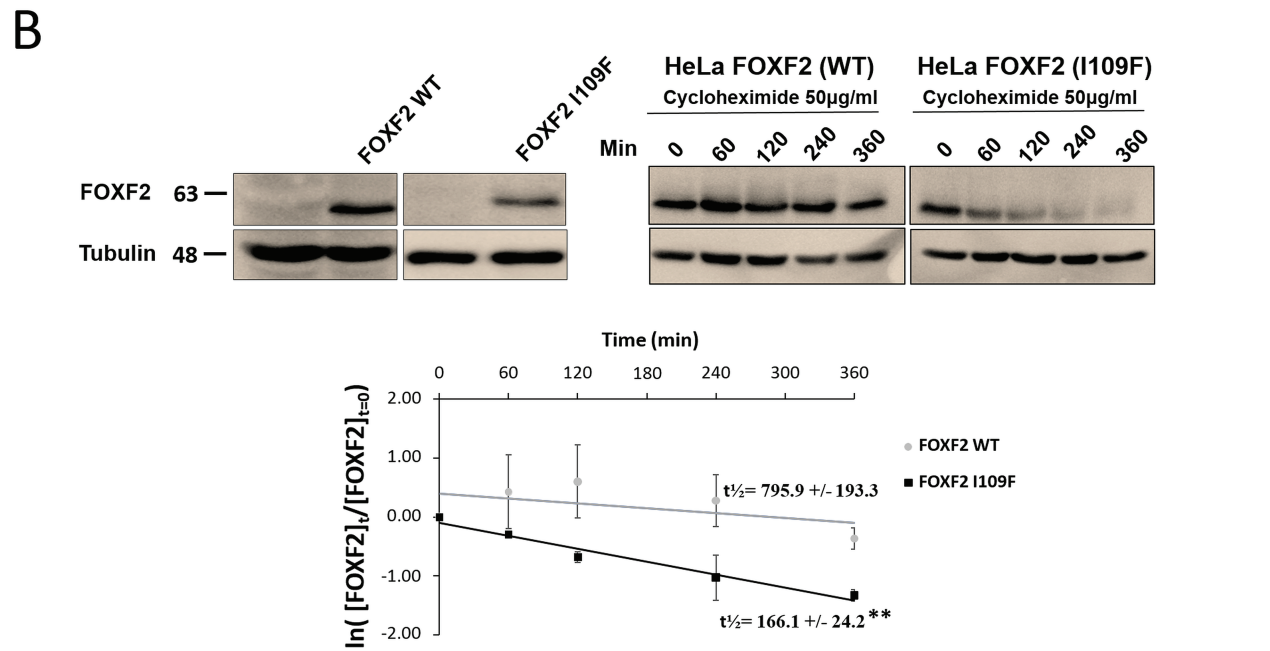

Figure 2. Conservation of FOXF2 I109 and stability of the F109 variant. (**A**) Comparison of the variant residue along with flanking amino acids in paralogs (upper panel) and orthologs (lower panel). (**B**) FOXF2 (WT)- and FOXF2 (I109F)-transfected HeLa cells were treated with cycloheximide (50 µg/ml) and then immunoblotting experiments were performed to measure FOXF2 protein levels after cycloheximide treatment for the indicated time points. Band intensities were normalized to α-tubulin then scaled to the 0 min cycloheximide time point. Error bars represent standard deviation (SD). The decay of FOXF2 followed first-order kinetics. The slope of the decay line was calculated by standard linear regression, and the protein half-life was determined accordingly. FOXF2 (WT), $t^{1/2}$ = 795.9 min; FOXF2 (I109F), $t^{1/2}$ = 166.1 min. $^{**}P < 0.01$ ($n = 3$; two-tailed *t*-test).

To understand the role of *Foxf2* in inner ear development, we analyzed previously generated *Foxf2*$^{-/-}$ mice, in which exon 1 (encoding the DNA-binding domain) of the gene is deleted (26). *Foxf2*$^{-/-}$ E18.5 day embryos were obtained as previously described (27). Microdissection and analysis of the cochlea reveal undercoiled and shortened cochleae in mutant animals, lacking approximately one full turn (Fig. 3A and B). Furthermore, a difference in auditory hair cell density in different regions of the cochlea between WT and mutant mice suggests an impaired convergent extension during development (Supplementary Material, Fig. S3). Immunostaining of the whole-mount cochlea with a hair cell-specific marker, Myo7a, reveals

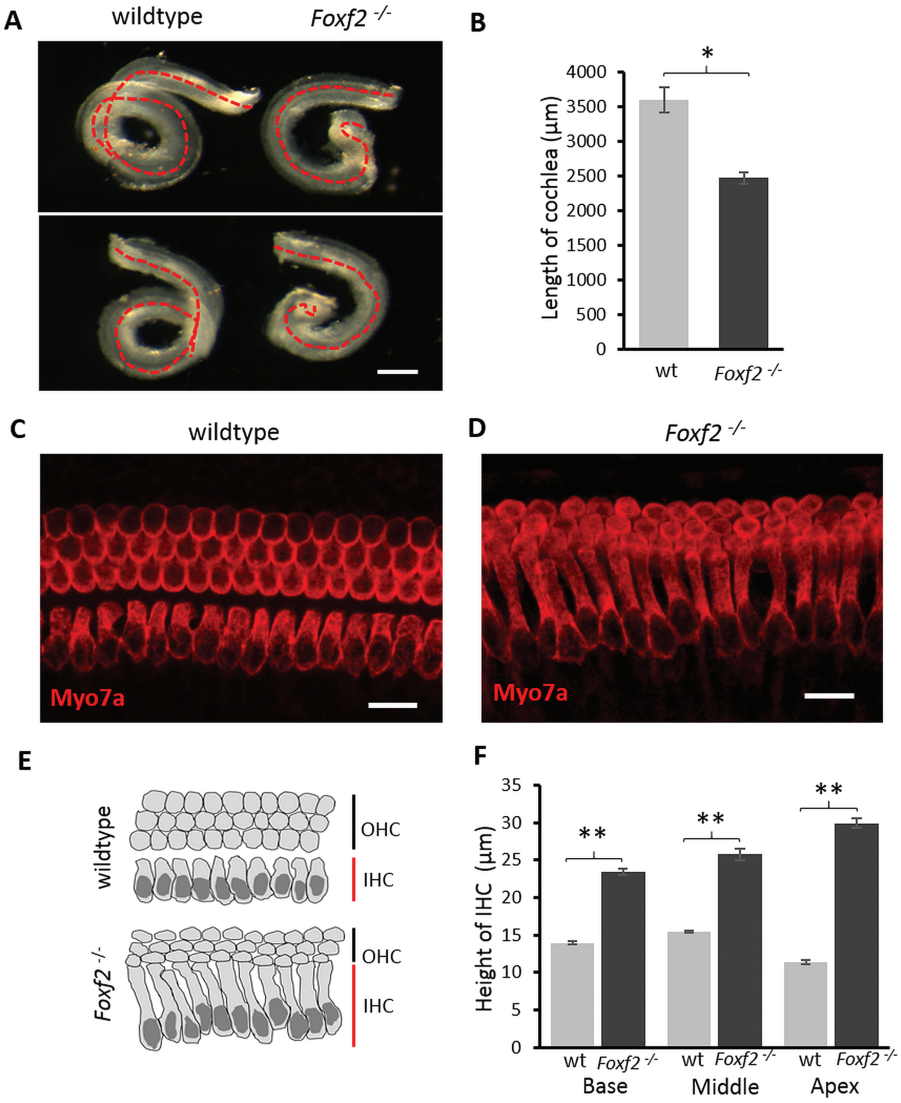

Figure 3. Cochlear length and hair cell morphology of *Foxf2*$^{-/-}$ mice. (**A**) Representative images from dissected cochleae at E18.5 for WT (left) and *Foxf2*$^{-/-}$ mice (right), showing an altered morphology and length in the mutant one. Scale bar: 300 µm. (**B**) Total length measurements of WT and *Foxf2*$^{-/-}$ E18.5 cochleae. Values are represented as average ± Standard Error of the Mean (SEM). $^{*}P < 0.05$ ($n = 3$ each genotype; two-tailed *t*-test). (**C** and **D**) Representative single plane confocal images showing the morphology of auditory hair cells from WT and *Foxf2*$^{-/-}$ whole-mount cochleae at E18.5. An anti-Myo7a (red) was used to stain auditory hair cell morphology. Scale bars c,d: 15 µm. (**E**) Schematic representation of hair cells morphology, depicting IHCs and OHCs, of WT and *Foxf2*$^{-/-}$ mice. (**F**) Height measurements of 100 IHCs in different parts of the cochlea are compared to WT (grey columns) and *Foxf2* $^{-/-}$ (black columns). Values are represented as the average ± SEM. $^{**}P < 0.01$ ($n = 4$ each genotype; two-tailed *t*-test).

an abnormally elongated cytoplasm of IHCs in *Foxf2*$^{-/-}$ mice (Fig. 3C–F; Supplementary Material, Fig. S4 and Videos S1 and S2).

To investigate the effect of *Foxf2* deficiency on the neuronal phenotype within the organ of Corti, we analyzed the hair cell innervation (z-stack images) in E18.5 whole-mount surface preparations of cochlea. Type I and type II spiral ganglion neuron (SGN) fibers connect with IHCs and OHCs, respectively. While the anti-neurofilament antibody stains both neuron types, the anti-peripherin antibody stains only type II neurons. Type II fibers invade the organ of Corti, turning toward the base to form three uniform, bundled tracks that run parallel between the Deiters' cells. Each fiber innervates 4–10 OHCs in WT animals (28). In *Foxf2*$^{-/-}$ mice, the regular arrangement of type II innervation is impaired and a striking reduction of the density of axons is observed throughout the organ of Corti (Fig. 4A and Supplementary Material, Fig. S4B). However, no difference in type I innervation or fasciculation is notable between WT and *Foxf2*$^{-/-}$ mice.

Planar polarity describes the coordinated polarization of cells or structures in the plane of a tissue. Development of planar polarity is necessary for normal hearing since stereociliary bundles are sensitive to vibrations only on a single plane (29). Planar polarization is also required for convergent extension, a polarized cellular movement that occurs during neural tube closure and cochlear extension. To assess the bundle orientation, we stained the bundles with phalloidin, a selective toxin that tightly binds F-actin. An anti-acetylated-α-tubulin antibody was used to identify the kinocilium. Morphology and stereociliary bundle orientation appear to be altered in the *Foxf2*$^{-/-}$ mice at age E18.5 compared to the WT (Fig. 4B and C; Supplementary Material, Fig. S5).

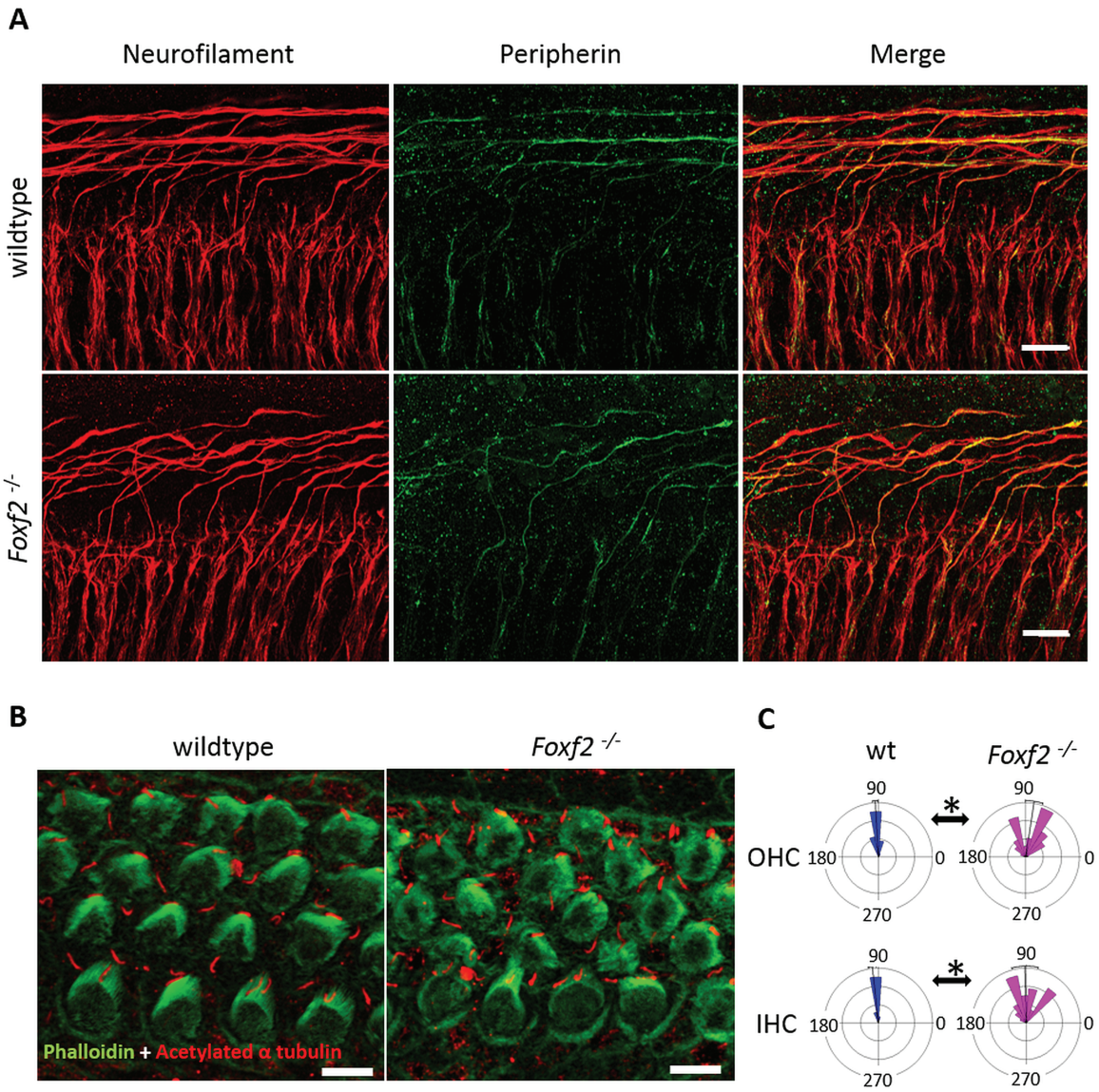

Figure 4. Innervation and planar cell polarity of hair cells in the cochleae of WT and *Foxf2*$^{-/-}$ mice at E18.5. (**A**) Representative images of the total innervation pattern (z-stack images) of E18.5 cochleae by immunostaining with anti-neurofilament (red) and type II SGN fibers stained with anti-peripherin (green) antibodies are shown for WT and *Foxf2*$^{-/-}$ mice. Scale bar:15 μm. (**B**) Representative single plane confocal images of apical stereocilia in cochlear whole mounts derived from WT and *Fofx2*$^{-/-}$ E18.5 mice. Anti-acetylated α-tubulin antibody was used to label the kinocilium (red), and Alexa Fluor 488 phalloidin (green) was used for F-actin staining of the stereocilia. Scale bar: 5 μm. (**C**) Representative results of individual stereociliary bundle orientations for IHCs and OHCs located in middle portion of the cochlea are presented as circular histograms for WT (blue) and *Foxf2*$^{-/-}$ (magenta) E18.5 embryos. Histograms represent stereociliary bundle orientation angles with 90 degrees indicating the normal angle formed between the longitudinal axis and mediolateral axis. Bundle orientation plots were generated using Oriana 4 circular graphing software. Deviations (>5 degrees) from the mediolateral axis were more frequent in stereociliary bundles from IHCs and OHCs of *Foxf2*$^{-/-}$ mice when compared to WT animals. The number of hair cells represented by each histogram is at least 50. Black bars and associated error bars show the mean ± SD of stereociliary bundle orientation. *$P < 0.05$ (cochleae derived from $n = 4$ WT and $n = 6$ knockouts, χ^2 test).

Foxf2 is a regulator for genes essential for cochlear development

To delineate the role Foxf2 plays in cochlear development, we evaluated the mRNA abundance of 17 genes (Supplementary Material, Table S7), known to cause inner ear anomalies when mutated, in fibroblasts from a homozygous mutant, a heterozygous mutant and an ethnicity-matched control. We sequenced the transcriptomes of these fibroblasts. This analysis yielded five differentially expressed genes (>1 log2 fold change): *EYA1*, *FGFR3* (MIM 134934), *HOXA1* (MIM 142955), *PAX3* and *ROR1* (Fig. 5A; Supplementary Material, Table S8). To validate observed changes in these genes, we used total RNA isolated form WT and *Foxf2*$^{-/-}$ E18.5 cochleae. As shown in Figure 5B, decreased mRNA levels for *Eya1* and *Pax3* were detected in the knockout mice. There was no difference for the other three genes evaluated.

Discussion

In this study, we identified a homozygous *FOXF2* variant underlying autosomal recessive incomplete partition type I anomaly of the cochlea and deafness in a family. The identified variant is novel, maps to an autozygous region (as expected with

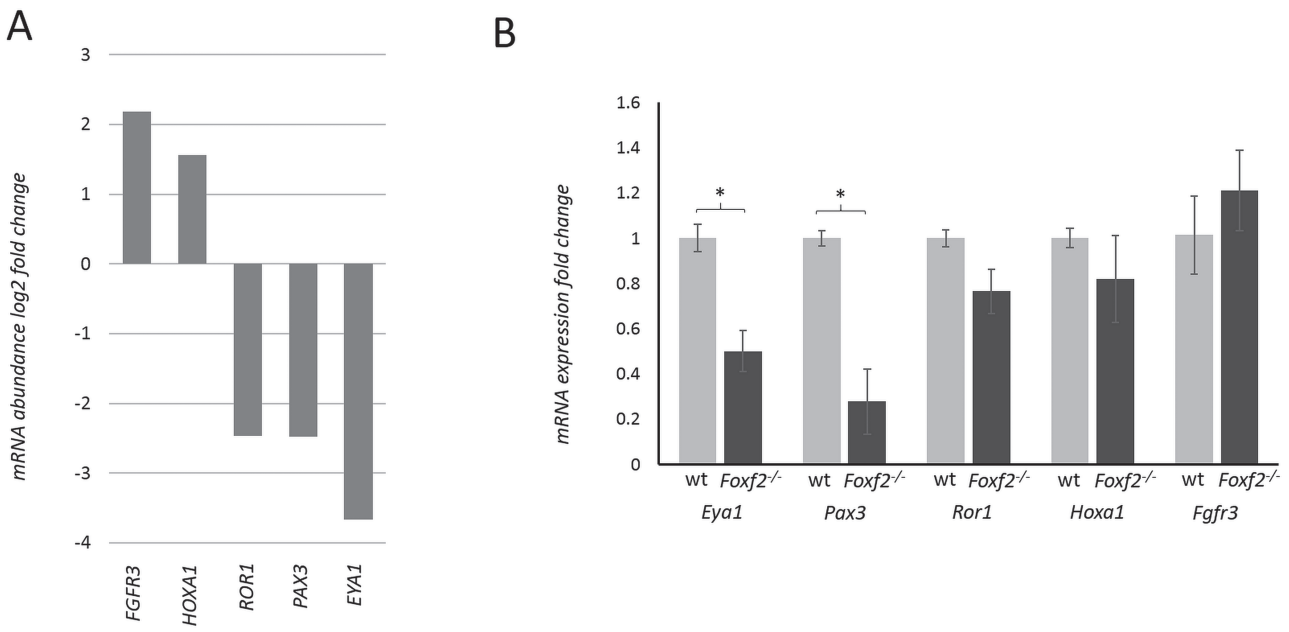

Figure 5. Transcriptome analysis of mutant human fibroblasts and mouse knockout gene expression studies. (**A**) Relative mRNA levels of five genes known to cause cochlear malformations in humans are shown from transcriptome sequencing of the fibroblasts from the proband (FOXF2 p.I109F) compared to a WT control. (**B**) Transcription levels of deregulated five genes shown in Fig. 5A were evaluated using quantitative polymerase chain reaction (qPCR) assays in the cochleae of E18.5 *Foxf2*$^{-/-}$ mice compared to those of WT animals. *Eya1* and *Pax3* gene expression values in *Foxf2*$^{-/-}$ mice were reduced [*$P < 0.05$ ($n = 6$, two-tailed *t*-test)], while there was no difference for *Fgfr3*, *Hoxa1* and *Ror1*.

parental consanguinity), alters a highly conserved residue and is indicated by multiple lines of *in silico* prediction analysis as having a damaging or deleterious effect on the protein. Remarkably, pathogenic variants involving the corresponding amino acids of the Fox domain in *FOXC1*, *FOXL2* and *FOXP3* have been reported to cause a variety of human disorders, highlighting the importance of this specific residue (21–24). *In vitro* studies show that the variant protein stability is reduced with a shortened half-life, supporting a causative role for the identified variant. Finally, *Foxf2* is expressed in the cochlea of developing and adult mice, and the mouse knockout model recapitulates the human cochlear phenotype.

FOXF2 is a transcription factor that is known to play a number of roles in embryonic development (13,25–27,30–34). It was originally identified as a transcription factor expressed in lungs and placenta (15). In addition to a Fox domain, FOXF2 (Uniprotkb ID: Q12947) contains two functionally redundant activation domains on the C-terminal side of the Fox domain (Fig. 1E) (35,36). Foxf2 is known to be a mesenchymal factor that controls epithelial proliferation and survival and closely interacts with several signaling pathways and genes, including Hedgehog, Wnt, FGFs and BMPs during embryonic development (26,27,31–34).

Human studies of *FOXF2* are limited. One study reported two common intronic variants (rs1711968 and rs732835) in *FOXF2* associated with non-syndromic cleft lip with or without cleft palate in an Asian population (37). Studies in mice have shown that Foxf2 is required for the development of craniofacial organs including the secondary palate, brain, intestine and possibly the anterior segment of the eye (26,27,30,31,38,39). *Foxf2*$^{-/-}$ mice that lack exon 1, which encodes the DNA-binding domain, die at birth (26). Some knockout mice present with cleft palate from E14 (the clefting phenotype penetrance is not complete and is one cause of death). Approximately 20% of knockout mice have a closed palate yet die shortly after birth; this may be due to the intestinal defects or other reasons, which remain unknown (30). Heterozygous mutant mice have normal survival (30). Another mouse model with a variant (W174R) affecting the Fox domain exhibits multiple anterior segment eye anomalies in both heterozygotes and homozygotes, and as expected the homozygotes do not survive (38). These studies indicate that mutations in the Foxf2 DNA-binding domain can result in a wide range of different murine phenotypes and homozygote mice present a severe phenotype that is always lethal.

Although *Foxf2* variants have been associated with diverse phenotypes in animal models, the proband in our study does not have features involving other organ systems previously reported to be associated with *Foxf2* dysfunction. Our *in vitro* experiments show that the p.I109F variant reduces the stability of FOXF2, but does not disrupt the protein entirely. We hypothesize that the p.I109F variant in FOXF2 reduces the availability of this transcription factor during embryonic development of the cochlea and leads to a cochlear anomaly with deafness. The reduction in the abundance of protein likely remains above some threshold for the development of other organs. Alternatively, there is limited redundancy of FOXF2 function during the cochlear development, whereas other FOX proteins can compensate for its absence in other organs.

Proper cochlear development requires the orchestrated action of numerous genes to make a tonotopically organized auditory organ. Cochlear elongation and cellular patterning during development have been proposed to be regulated by a developmentally conserved process referred to as convergence and extension, whereby cells within a plane rearrange from a shorter and wider domain to one that is longer and narrower (40,41). Shortened cochleae with defects in cellular patterning have been shown in mutant mice that model planar cell polarity (PCP) genes (42–44). While the *Foxf2* knockout mouse model in this study shows disturbed PCP in the inner ear sensory cells at

an embryonic stage, it remains unknown if PCP defects persist in adult mice.

Expression of *Eya1* and *Pax3* is reduced in the cochlea of *Foxf2* knockout mice. *Eya1* codes for a transcriptional activator, which plays a role in developing kidney, branchial arches, eye and ear. The patterning defects of cochlear sensory cells with disrupted innervation, as well as shortened and malformed cochlea, have been reported in mutant *Eya1* mouse models (45,46). Similarities of the cochlear phenotypes detected in mutant *Eya1* and *Foxf2* mouse models suggest that reduced *Eya1* expression in the cochleae of *Foxf2* knockout mice explains, at least in part, the cochlear malformation and hearing loss. Pax3 is a transcription factor that consists of a paired-box homeodomain and plays a role in the downstream target of Wnt signaling in premigratory neural crest cells (47). Mouse knockouts for *Pax3* present with cochlear malformation with some variability (48).

In conclusion, we present Foxf2 as a crucial protein during the cochlear development, which controls the expression of multiple genes including *Eya1* and *Pax3*. Dysfunction of Foxf2 leads to cochlear malformations and deafness in humans and mice.

Materials and Methods

Human subjects

This study was approved by the ethics committee of Ankara University in Turkey (012413) and the institutional review board at the University of Miami in the USA (20081138). A signed informed consent form was obtained from each participant or, in the case of a minor, from parents. This study was performed in a Turkish family with a proband presenting with profound SNHL and a cochlear anomaly. Clinical evaluations were performed by an otorhinolaryngologist, a geneticist, an ophthalmologist and a radiologist and included a review of symptoms, past medical history and family history; review of systems; a physical examination including otoscopy and ophthalmoscopy; and a computerized tomography scan of the temporal bone. DNA from the proband, both parents and unaffected sibling was extracted from blood samples via standard methods.

Whole exome and genome sequencing

WES was performed using our previously published protocol (49). Agilent SureSelect Human All Exon V6 was used for the capture. Variants were filtered via Genesis 2.0 platform (https://www.genesis-app.com/). We analyzed the trio/quad data under homozygous recessive, compound heterozygous and *de novo* models. For the variant allele frequency filtering, EVS (http://evs.gs.washington.edu/EVS/), gnomAD (http://gnomad.broadinstitute.org/) and dbSNP (https://www.ncbi.nlm.nih.gov/projects/SNP/) databases were used in addition to our internal WES database that contains >4000 exomes from different ethnicities, including >1000 Turkish individuals. Minor allele frequency thresholds of 0.005 for recessive and 0.0005 for dominant variants were used (50). GERP of >2 (http://mendel.stanford.edu/SidowLab/downloads/gerp/index.html) was used for conservation (51). We also filtered missense variants by using the criteria of DANN score of >0.9 (https://cbcl.ics.uci.edu/public_data/DANN/), CADD score of >20 (https://cadd.gs.washington.edu/), damaging for SIFT (http://sift.jcvi.org/) and FATHMM (http://fathmm.biocompute.org.uk/), high impact for MutationAssessor (http://mutationassessor.org/r3/) and disease causing for MutationTaster (http://www.mutationtaster.org/). Additionally, American College of Medical Genetics and Genomics guidelines were considered for the variant interpretation (52). XHMM and CoNIFER were used for the detection of the copy number variants (CNVs) (53,54). Sanger sequencing was performed for the confirmation and co-segregation of the variant with hearing loss. Enlis Genome Research software (https://www.enlis.com/) was used to identify homozygous regions from WES data.

Whole genome sequencing was performed in the entire family (I:1, I:2, II:1 and II:2) by using a BGISEQ-500 instrument with paired-end 100 bp protocol (55). Reads were mapped by Burrows–Wheeler Aligner to the human reference genome version NCBI build37/hg19, while Genome Analysis Toolkit was used for variant calling (56, 57). CNVnator was used for CNVs and BreakDancer for structural variants (58,59).

FOXF2 subcellular localization and abundance

An open reading frame expression clone for C-terminus (hemagglutinin) HA-tagged WT *FOXF2* (NM_001452.1) was purchased from GeneCopoeia (EX-M0875-M07). The mutant variant was generated using QuikChange® Site-Directed Mutagenesis Kit (Agilent Technologies, Santa Clara, CA), primer pairs SDM_FOXF2_F, SDM_FOXF2_R (Supplementary Material, Table S9) and the vector containing WT *FOXF2*. To investigate the subcellular localization of WT and mutant FOXF2, COS-7 cells grown on coverslips placed in six well plates were transfected. HA-tagged WT and mutant FOXF2-HA-encoding constructs were used as transfection vectors. Lipofectamine 3000 (Invitrogen, Carlsbad, CA) was the transfection agent utilized following the manufacturer's standard instructions. At 48 h posttransfection, cells were washed with phosphate buffered saline (PBS) and fixed with 4% paraformaldehyde (PFA) in PBS. Cells were permeabilized with 0.5% Triton X-100 in PBS for 20 min, blocked with 5% bovine serum albumin (BSA), and then an anti-HA-tag rabbit monoclonal antibody (Cell Signaling Technology, Danvers, MA) was applied for 1 h. Specimens were washed with PBS, then anti-rabbit Alexa Fluor 488 and DAPI (4′,6-diamidino-2-phenylindole) were applied. Specimens were washed again with PBS and mounted in Fluorescence Mounting Medium (Dako, Santa Clara, CA).

Protein stability

HA-tagged FOXF2 (WT) and FOXF2 (I109F) plasmids were transfected in HeLa cells using the Lipofectamine2000® reagent (Invitrogen), per the manufacturer's instructions. Cells were transfected for 48 h then were treated with cycloheximide (50 µg/ml) for 0–6 h. For immunoblotting experiments, the cells were first rinsed 2 times with 5 ml of PBS. Cells then were gently scraped and harvested at different time points in 50 µl of lysis buffer (IGEPAL® CA-630, 0.05 M Tris pH 8.0, 0.15 M NaCl, 1 mM PMSF, 0.05% protease inhibitor cocktail) and then incubated on ice for 15 min. Next, cells were centrifuged at 14,000*g* for 5 min at 4°C. The supernatants were transferred to a new tube, quantified, denatured at 95°C for 5 min and size-separated on an 8% SDS-PAGE gel. HA-probe-tagged FOXF2 proteins were detected by a commercial rabbit anti-HA probe antibody (Y-11) (Santa Cruz Biotechnology, Dallas, Texas) 1:5000 and mouse anti-α-tubulin (Santa Cruz Biotechnology) 1:2000. The band intensities were quantified with ImageJ software. A two-tailed Student's *t*-test was applied to determine statistical significance using slopes

over the time of cycloheximide treatment. Three independent transfection experiments were carried out to determine the rates of decay of FOXF2 proteins.

Human fibroblast cells

Fibroblasts were grown in Dulbecco's Modified Eagle Medium supplemented with 20% fetal bovine serum from the skin biopsies performed on the proband (II:1) and unaffected mother (I:2). Additionally, a FOXF2 WT Turkish person's fibroblast cell culture was used as a control. RNA extraction and purification were performed using TRIzol (Invitrogen) and RNAeasy Mini Kit (Qiagen, Venlo, Netherlands), respectively.

RNA-Seq analysis

We sequenced the transcriptomes of fibroblasts from the proband (II:1), unaffected mother (I:2) and a control fibroblast cell culture in triplicates.

Total RNA was quantified and qualified using the Agilent Bioanalyzer to have an RNA integrity score set to 9. For RNA preparations, 1000 ng of total RNA was used as input for the Illumina TruSeq Total RNA Library Prep Kit with Ribo-Zero. Each sample had an incorporated unique barcode to allow for multiplexing. For total RNA libraries, approximately 60 million raw reads were generated in a 2 × 100 paired-end sequencing run.

Raw sequence data from the Illumina HiSeq2500 were processed by the on-instrument Real-Time Analysis software (v.1.8) to base call files. These were converted to demultiplexed FASTQ files with the Illumina supplied scripts in the bcl2fastq software (v1.8.4). The quality of the reads was determined with FastQC software (http://www.bioinformatics.babraham.ac.uk/projects/fastqc/) for per base sequence quality, duplication rates and overrepresented k-mers. Illumina adapters were trimmed from the ends of the reads using the Trim Galore! package (http://www.bioinformatics.babraham.ac.uk/projects/trim_galore/). Reads were aligned to the human reference genome (hg19) with the STAR aligner (v2.5.0a) (60). Gene count quantification for total RNA was performed using the GeneCounts function within STAR against the GENCODE v19 transcript file.

Gene count data were put into edgeR and DESeq2 software for differential expression analysis (61–63). Briefly, gene counts were normalized against total aligned reads for each sample to generate an expression value (counts per million) for each gene in each sample. Given the relatively small sample sizes per group, for comparison (n = 3 in each group), the exact text implemented in edgeR and DESeq2 were used to determine differential expression including a false discovery rate P-value.

Mouse strains

WT C57Bl/6 mice were bred and maintained at the University of Miami. At weaning age, mice were housed 2–4 per cage in a room with a 12 h light–dark cycle (lights on at 7 AM, off at 7 PM) with access to food and water *ad lib*. All procedures were approved by the University of Miami Institutional Animal Care and Use Committee and followed the National Institute of Health (NIH) guidelines, 'Using Animals in Intramural Research'.

The *Foxf2* knockout strain carrying the null allele was bred and maintained at the University of Gothenburg animal facility in agreement with Swedish animal welfare legislation and animal research ethical permit Dnr 21-2014 held by P.C. (26). Since the creation of the null allele, it has been maintained in heterozygous state by routine breeding and homozygous embryos obtained by crossing heterozygotes.

RT-PCR

To determine the expression of *Foxf2* in different tissues, lung, liver, hippocampus, cortex, kidney and cochlea were dissected from P15 WT mice. In addition, cochlear expression of *Foxf2* was analyzed in E17.5 and P0 mice. Total RNA was isolated with TRIzol reagent (Invitrogen) according to manufacturer's instructions. Prior to reverse transcription, RNA samples were treated with rDNAse I (DNA-free kit, Applied Biosystems, Foster City, CA). cDNA was synthetized using qScript XLT cDNA SuperMix (Quanta Biosciences, Beverly, MA). The primers used to amplify a 201 bp fragment of the *Foxf2* transcript (m_Foxf2_F; m_Foxf2_R) and 129 bp fragment of *Gapdh* (m_Gapdh_F; m_Gapdh_R) are listed in Supplementary Material, Table S9.

Quantitative RT-PCR analysis

Total RNA was isolated from fixed E18.5 cochleae from WT and mutant mice using a miRNeasy FFPE Kit (Qiagen) according to manufacturer's instructions. Prior to reverse transcription, RNA samples were treated with rDNAse I (DNA-free kit, Applied Biosystems). cDNA was synthetized using qScript XLT cDNA SuperMix (Quanta Biosciences). Primers used for detecting *Ror1* (m_Ror1_F; m_Ror1_R), *Eya1* (m_Eya1_F; m_Eya1_R) and *Gapdh* (m_Gapdh_F; m_Gapdh_R) (used as the reference gene) with SYBR Green are listed in Supplementary Material, Table S9. Furthermore, TaqMan assays for *Fgfr3* (Mm00433294_m1), *Pax3* (Mm00435493_m1), *Hoxa1* (Mm00439359_m1), *Eya1* (Mm00438796_m1) and *Gapdh* (Mm99999915_g1) were used to detect gene expression levels.

Immunofluorescence

Embryo heads were fixed in 4% buffered PFA. The tympanic bullae containing the cochleae were dissected from E18.5 WT and mutant embryos under the microscope and locally perfused with 4% PFA through the round and oval windows. Samples were kept in 4% PFA at 4°C overnight and rinsed in 1× PBS. The cochleae were permeabilized with 0.25% Triton X-100 and blocked in 5% BSA for 1 h at room temperature, followed by overnight incubation at 4°C with primary antibodies. A mouse anti-Myo7a monoclonal antibody (MYO7A 138–1, Developmental Studies Hybridoma Bank at the University of Iowa), a chicken anti-neurofilament polyclonal antibody (AB5539, Millipore-Sigma, Burlington, MA), a rabbit anti-peripherin polyclonal antibody (AB1530, MilliporeSigma) and an anti-acetylated α-tubulin mouse monoclonal (T7451, Sigma-Aldrich, St. Louis, MO) were utilized as a primary antibody. Co-staining was performed with Alexa Fluor 488 phalloidin (Thermo Fisher, Waltham, MA, A12379) and DAPI (Calbiochem, San Diego, CA) to stain actin and nuclear DNA, respectively. Images were captured with a Zeiss LSM710 confocal microscope.

Quantification of hair cell planar polarity

To measure hair cell planar polarity, a previously described protocol was followed (64). Briefly, the organ of Corti was imaged by confocal microscopy at 3 positions corresponding to 25%, 50% and 75% of the length of the cochlea measured from the base. The orientation of individual hair cells was measured using the ImageJ (NIH) angle measurement tool. The short arm of

each angle was drawn from the α-acetylated tubulin-labeled kinocilium and across the center of the hair cell. The long arm of each angle was drawn parallel to three adjacent hair cells within the same row. Absolute measurements of auditory hair cell orientation were assembled as circular histograms using Oriana 4 circular graphing software (Kovach Computing Services, Pentraeth, UK). These analyses were completed for each genotype at the three cochlear positions.

Statistical analysis

The statistical analysis and the sample sizes (n) are listed in each figure legend. The mouse data were analyzed using a t-test, except for the PCP study, for which the auditory hair cell orientation statistical significance was calculated by χ^2 test using Oriana 4 (Kovach Computing Services).

Supplementary Material

Supplementary Material is available at *HMG* online.

Conflict of Interest statement. None declared.

Funding

National Institutes of Health (R01DC009645 and R01DC012836 to M.T.); Swedish Medical Research Council (VR-M); Swedish Cancer Foundation (P.C.); and Microsoft Genomics for Research (G.B.).

References

1. Morton, C.C. and Nance, W.E. (2006) Newborn hearing screening—a silent revolution. *N. Engl. J. Med.*, **354**, 2151–2164.
2. Jackler, R.K., Luxford, W.M. and House, W.F. (1987) Congenital malformations of the inner ear: a classification based on embryogenesis. *Laryngoscope*, **97**, 2–14.
3. Adibelli, Z.H., Isayeva, L., Koc, A.M., Catli, T., Adibelli, H. and Olgun, L. (2017) The new classification system for inner ear malformations: the INCAV system. *Acta Otolaryngol.*, **137**, 246–252.
4. Sennaroglu, L. and Saatci, I. (2002) A new classification for cochleovestibular malformations. *Laryngoscope*, **112**, 2230–2241.
5. Wu, D.K. and Kelley, M.W. (2012) Molecular mechanisms of inner ear development. *Cold Spring Harb. Perspect. Biol.*, **4**, a008409.
6. Diaz-Horta, O., Abad, C., Sennaroglu, L., Foster, J. 2nd, DeSmidt, A., Bademci, G., Tokgoz-Yilmaz, S., Duman, D., Cengiz, F.B., Grati, M. *et al.* (2016) ROR1 is essential for proper innervation of auditory hair cells and hearing in humans and mice. *Proc. Natl. Acad. Sci. U. S. A.*, **113**, 5993–5998.
7. Tekin, M., Hismi, B.O., Fitoz, S., Ozdağ, H., Cengiz, F.B., Sirmaci, A., Aslan, I., Inceoğlu, B., Yüksel-Konuk, E.B., Yilmaz, S.T., Yasun, O. and Akar, N. (2007) Homozygous mutations in fibroblast growth factor 3 are associated with a new form of syndromic deafness characterized by inner ear agenesis, microtia, and microdontia. *Am. J. Hum. Genet.*, **80**, 338–344.
8. Bosman, E.A., Penn, A.C., Ambrose, J.C., Kettleborough, R., Stemple, D.L. and Steel, K.P. (2005) Multiple mutations in mouse Chd7 provide models for CHARGE syndrome. *Hum. Mol. Genet.*, **14**, 3463–3476.
9. Dror, A.A., Brownstein, Z. and Avraham, K.B. (2011) Integration of human and mouse genetics reveals pendrin function in hearing and deafness. *Cell. Physiol. Biochem.*, **28**, 535–544.
10. Whitfield, T.T. (2015) Development of the inner ear. *Curr. Opin. Genet. Dev.*, **32**, 112–118.
11. Weigel, D., Bellen, H.J., Jürgens, G. and Jäckle, H. (1989) Primordium specific requirement of the homeotic gene fork head in the developing gut of the *Drosophila* embryo. *Rouxs Arch. Dev. Biol.*, **198**, 201–210.
12. Golson, M.L. and Kaestner, K.H. (2016) Fox transcription factors: from development to disease. *Development*, **143**, 4558–4570.
13. Hannenhalli, S. and Kaestner, K.H. (2009) The evolution of Fox genes and their role in development and disease. *Nat. Rev. Genet.*, **10**, 233–240.
14. Kaestner, K.H., Katz, J., Liu, Y., Drucker, D.J. and Schütz, G. (1999) Inactivation of the winged helix transcription factor HNF3alpha affects glucose homeostasis and islet glucagon gene expression in vivo. *Genes Dev.*, **13**, 495–504.
15. Pierrou, S., Hellqvist, M., Samuelsson, L., Enerbäck, S. and Carlsson, P. (1994) Cloning and characterization of seven human forkhead proteins: binding site specificity and DNA bending. *EMBO J.*, **13**, 5002–5012.
16. Nishimura, D.Y., Swiderski, R.E., Alward, W.L., Searby, C.C., Patil, S.R., Bennet, S.R., Kanis, A.B., Gastier, J.M., Stone, E.M. and Sheffield, V.C. (1998) The forkhead transcription factor gene FKHL7 is responsible for glaucoma phenotypes which map to 6p25. *Nat. Genet.*, **19**, 140–147.
17. Crisponi, L., Deiana, M., Loi, A., Chiappe, F., Uda, M., Amati, P., Bisceglia, L., Zelante, L., Nagaraja, R., Porcu, S. *et al.* (2001) The putative forkhead transcription factor FOXL2 is mutated in blepharophimosis/ptosis/epicanthus inversus syndrome. *Nat. Genet.*, **27**, 159–166.
18. Lai, C.S., Fisher, S.E., Hurst, J.A., Levy, E.R., Hodgson, S., Fox, M., Jeremiah, S., Povey, S., Jamison, D.C., Green, E.D., Vargha-Khadem, F., and Monaco, A.P. (2000) The SPCH1 region on human 7q31: genomic characterization of the critical interval and localization of translocations associated with speech and language disorder. *Am. J. Hum. Genet.*, **67**, 357–368.
19. Chatila, T.A., Blaeser, F., Ho, N., Lederman, H.M., Voulgaropoulos, C., Helms, C. and Bowcock, A.M. (2000) JM2, encoding a fork head-related protein, is mutated in X-linked autoimmunity–allergic disregulation syndrome. *J. Clin. Invest.*, **106**, R75–R81.
20. Enerbäck, S., Nilsson, D., Edwards, N., Heglind, M., Alkanderi, S., Ashton, E., Deeb, A., Kokash, F.E.B., Bakhsh, A.R.A., Van't Hoff, W. *et al.* (2018) Acidosis and deafness in patients with recessive mutations in FOXI1. *J. Am. Soc. Nephrol.*, **29**, 1041–1048.
21. Mears, A.J., Jordan, T., Mirzayans, F., Dubois, S., Kume, T., Parlee, M., Ritch, R., Koop, B., Kuo, W.L., Collins, C. *et al.* (1998) Mutations of the forkhead/winged-helix gene, FKHL7, in patients with Axenfeld-Rieger anomaly. *Am. J. Hum. Genet.*, **63**, 1316–1328.
22. Nallathambi, J., Laissue, P., Batista, F., Benayoun, B.A., Lesaffre, C., Moumné, L., Pandaranayaka, P.E., Usha, K., Krishnaswamy, S., Sundaresan, P. and Veitia, R.A. (2008) Differential functional effects of novel mutations of the transcription factor FOXL2 in BPES patients. *Hum. Mutat.*, **29**, E123–E131.
23. Or, S.F., Tong, M.F., Lo, F.M. and Lam, T.S. (2006) Three novel FOXL2 gene mutations in Chinese patients with blepharophimosis–ptosis–epicanthus inversus syndrome. *Chin. Med. J. (Engl.)*, **119**, 49–52.

24. Passerini, L., Olek, S., Di Nunzio, S., Barzaghi, F., Hambleton, S., Abinun, M., Tommasini, A., Vignola, S., Cipolli, M., Amendola, M. *et al.* (2011) Forkhead box protein 3 (FOXP3) mutations lead to increased TH17 cell numbers and regulatory T-cell instability. *J. Allergy Clin. Immunol.*, **128**, 1376–1379e.1.
25. Aitola, M., Carlsson, P., Mahlapuu, M., Enerbäck, S. and Pelto-Huikko, M. (2000) Forkhead transcription factor FoxF2 is expressed in mesodermal tissues involved in epithelio-mesenchymal interactions. *Dev. Dyn.*, **218**, 136–149.
26. Reyahi, A., Nik, A.M., Ghiami, M., Gritli-Linde, A., Ponten, F., Johansson, B.R. and Carlsson, P. (2015) Foxf2 is required for brain pericyte differentiation and development and maintenance of the blood–brain barrier. *Dev. Cell*, **34**, 19–32.
27. Nik, A.M., Johansson, J.A., Ghiami, M., Reyahi, A. and Carlsson, P. (2016) Foxf2 is required for secondary palate development and Tgfβ signaling in palatal shelf mesenchyme. *Dev. Biol.*, **415**, 14–23.
28. Barclay, M., Ryan, A.F. and Housley, G.D. (2011) Type I vs type II spiral ganglion neurons exhibit differential survival and neuritogenesis during cochlear development. *Neural Dev.*, **6**, 33.
29. Dabdoub, A., Donohue, M.J., Brennan, A., Wolf, V., Montcouquiol, M., Sassoon, D.A., Hseih, J.C., Rubin, J.S., Salinas, P.C. and Kelley, M.W. (2003) Wnt signaling mediates reorientation of outer hair cell stereociliary bundles in the mammalian cochlea. *Development*, **130**, 2375–2384.
30. Wang, T., Tamakoshi, T., Uezato, T., Shu, F., Kanzaki-Kato, N., Fu, Y., Koseki, H., Yoshida, N., Sugiyama, T. and Miura, N. (2003) Forkhead transcription factor Foxf2 (LUN)-deficient mice exhibit abnormal development of secondary palate. *Dev. Biol.*, **259**, 83–94.
31. Ormestad, M., Astorga, J., Landgren, H., Wang, T., Johansson, B.R., Miura, N. and Carlsson, P. (2006) Foxf1 and Foxf2 control murine gut development by limiting mesenchymal Wnt signaling and promoting extracellular matrix production. *Development*, **133**, 833–843.
32. Nik, A.M., Reyahi, A., Pontén, F. and Carlsson, P. (2013) Foxf2 in intestinal fibroblasts reduces numbers of Lgr5(+) stem cells and adenoma formation by inhibiting Wnt signaling. *Gastroenterology*, **144**, 1001–1011.
33. Xu, J., Liu, H., Lan, Y., Aronow, B.J., Kalinichenko, V.V. and Jiang, R. (2016) A Shh-Foxf-Fgf18-Shh molecular circuit regulating palate development. *PLoS Genet.*, **12**, e1005769.
34. Everson, J.L., Fink, D.M., Yoon, J.W., Leslie, E.J., Kietzman, H.W., Ansen-Wilson, L.J., Chung, H.M., Walterhouse, D.O., Marazita, M.L. and Lipinski, R.J. (2017) Sonic hedgehog regulation of Foxf2 promotes cranial neural crest mesenchyme proliferation and is disrupted in cleft lip morphogenesis. *Development*, **144**, 2082–2091.
35. Hellqvist, M., Mahlapuu, M., Blixt, A., Enerbäck, S. and Carlsson, P. (1998) The human forkhead protein FREAC-2 contains two functionally redundant activation domains and interacts with TBP and TFIIB. *J. Biol. Chem.*, **273**, 23335–23343.
36. Hellqvist, M., Mahlapuu, M., Samuelsson, L., Enerbäck, S. and Carlsson, P. (1996) Differential activation of lung-specific genes by two forkhead proteins, FREAC-1 and FREAC-2. *J. Biol. Chem.*, **271**, 4482–4490.
37. Bu, L., Chen, Q., Wang, H., Zhang, T., Hetmanski, J.B., Schwender, H., Parker, M., Chou, Y.H., Yeow, V., Chong, S.S. *et al.* (2015) Novel evidence of association with nonsyndromic cleft lip with or without cleft palate was shown for single nucleotide polymorphisms in FOXF2 gene in an Asian population. *Birth Defects Res. A Clin. Mol. Teratol.*, **103**, 857–862.
38. McKeone, R., Vieira, H., Gregory-Evans, K., Gregory-Evans, C.Y. and Denny, P. (2011) Foxf2: a novel locus for anterior segment dysgenesis adjacent to the Foxc1 gene. *PLoS One*, **6**, e25489.
39. Hoffmann, A.D., Yang, X.H., Burnicka-Turek, O., Bosman, J.D., Ren, X., Steimle, J.D., Vokes, S.A., McMahon, A.P., Kalinichenko, V.V. and Moskowitz, I.P. (2014) Foxf genes integrate tbx5 and hedgehog pathways in the second heart field for cardiac septation. *PLoS Genet.*, **10**, e1004604.
40. Tada, M. and Heisenberg, C.P. (2012) Convergent extension: using collective cell migration and cell intercalation to shape embryos. *Development*, **139**, 3897–3904.
41. Driver, E.C., Northrop, A. and Kelley, M.W. (2017) Cell migration, intercalation and growth regulate mammalian cochlear extension. *Development*, **144**, 3766–3776.
42. Montcouquiol, M., Rachel, R.A., Lanford, P.J., Copeland, N.G., Jenkins, N.A. and Kelley, M.W. (2003) Identification of Vangl2 and Scrb1 as planar polarity genes in mammals. *Nature*, **423**, 173–177.
43. Wang, J., Mark, S., Zhang, X., Qian, D., Yoo, S.J., Radde-Gallwitz, K., Zhang, Y., Lin, X., Collazo, A., Wynshaw-Boris, A. and Chen, P. (2005) Regulation of polarized extension and planar cell polarity in the cochlea by the vertebrate PCP pathway. *Nat. Genet.*, **37**, 980–985.
44. Wang, J., Hamblet, N.S., Mark, S., Dickinson, M.E., Brinkman, B.C., Segil, N., Fraser, S.E., Chen, P., Wallingford, J.B. and Wynshaw-Boris, A. (2006) Dishevelled genes mediate a conserved mammalian PCP pathway to regulate convergent extension during neurulation. *Development*, **133**, 1767–1778.
45. Zou, D., Erickson, C., Kim, E.H., Jin, D., Fritzsch, B. and Xu, P.X. (2008) Eya1 gene dosage critically affects the development of sensory epithelia in the mammalian inner ear. *Hum. Mol. Genet.*, **17**, 3340–3356.
46. Ahmed, M., Xu, J. and Xu, P.X. (2012) EYA1 and SIX1 drive the neuronal developmental program in cooperation with the SWI/SNF chromatin-remodeling complex and SOX2 in the mammalian inner ear. *Development*, **139**, 1965–1977.
47. Freyer, L., Aggarwal, V. and Morrow, B.E. (2011) Dual embryonic origin of the mammalian otic vesicle forming the inner ear. *Development*, **138**, 5403–5414.
48. Buckiová, D. and Syka, J. (2004) Development of the inner ear in Splotch mutant mice. *Neuroreport*, **15**, 2001–2005.
49. Bademci, G., Foster, J. 2nd, Mahdieh, N., Bonyadi, M., Duman, D., Cengiz, F.B., Menendez, I., Diaz-Horta, O., Shirkavand, A., Zeinali, S. *et al.* (2016) Comprehensive analysis via exome sequencing uncovers genetic etiology in autosomal recessive nonsyndromic deafness in a large multiethnic cohort. *Genet. Med.*, **18**, 364–371.
50. Shearer, A.E., Eppsteiner, R.W., Booth, K.T., Ephraim, S.S., Gurrola, J. 2nd, Simpson, A., Black-Ziegelbein, E.A., Joshi, S., Ravi, H., Giuffre, A.C. *et al.* (2014) Utilizing ethnic-specific differences in minor allele frequency to recategorize reported pathogenic deafness variants. *Am. J. Hum. Genet.*, **95**, 445–453.
51. Cooper, G.M., Stone, E.A., Asimenos, G., NICS Comparative Sequencing Program, Green, E.D., Batzoglou, S. and Sidow, A. (2005) Distribution and intensity of constraint in mammalian genomic sequence. *Genome Res.*, **15**, 901–913.

52. Richards, S., Aziz, N., Bale, S., Bick, D., Das, S., Gastier-Foster, J., Grody, W.W., Hegde, M., Lyon, E., Spector, E. *et al.* (2015) Standards and guidelines for the interpretation of sequence variants: a joint consensus recommendation of the American College of Medical Genetics and Genomics and the Association for Molecular Pathology. *Genet. Med.*, **17**, 405–424.
53. Bademci, G., Diaz-Horta, O., Guo, S., Duman, D., Van Booven, D., Foster, J. 2nd, Cengiz, F.B., Blanton, S. and Tekin, M. (2014) Identification of copy number variants through whole-exome sequencing in autosomal recessive nonsyndromic hearing loss. *Genet. Test. Mol. Biomarkers*, **18**, 658–661.
54. Quang, D., Chen, Y. and Xie, X. (2015) DANN: a deep learning approach for annotating the pathogenicity of genetic variants. *Bioinformatics*, **31**, 761–763.
55. Huang, J., Liang, X., Xuan, Y., Geng, C., Li, Y., Lu, H., Qu, S., Mei, X., Chen, H., Yu, T. *et al.* (2017) A reference human genome dataset of the BGISEQ-500 sequencer. *Gigascience*, **6**, 1–9.
56. Li, H. and Durbin, R. (2010) Fast and accurate long-read alignment with Burrows–Wheeler transform. *Bioinformatics*, **26**, 589–595.
57. McKenna, A., Hanna, M., Banks, E., Sivachenko, A., Cibulskis, K., Kernytsky, A., Garimella, K., Altshuler, D., Gabriel, S., Daly, M. and DePristo, M.A. (2010) The Genome Analysis Toolkit: a MapReduce framework for analyzing next-generation DNA sequencing data. *Genome Res.*, **20**, 1297–1303.
58. Abyzov, A., Urban, A.E., Snyder, M. and Gerstein, M. (2011) CNVnator: an approach to discover, genotype, and characterize typical and atypical CNVs from family and population genome sequencing. *Genome Res.*, **21**, 974–984.
59. Chen, K., Wallis, J.W., McLellan, M.D., Larson, D.E., Kalicki, J.M., Pohl, C.S., McGrath, S.D., Wendl, M.C., Zhang, Q., Locke, D.P. *et al.* (2009) BreakDancer: an algorithm for high-resolution mapping of genomic structural variation. *Nat. Methods*, **6**, 677–681.
60. Dobin, A., Davis, C.A., Schlesinger, F., Drenkow, J., Zaleski, C., Jha, S., Batut, P., Chaisson, M. and Gingeras, T.R. (2013) STAR: ultrafast universal RNA-seq aligner. *Bioinformatics*, **29**, 15–21.
61. Robinson, M.D., McCarthy, D.J. and Smyth, G.K. (2010) edgeR: a Bioconductor package for differential expression analysis of digital gene expression data. *Bioinformatics*, **26**, 139–140.
62. Love, M.I., Huber, W. and Anders, S. (2014) Moderated estimation of fold change and dispersion for RNA-seq data with DESeq2. *Genome Biol.*, **15**, 550.
63. Hardcastle, T.J. and Kelly, K.A. (2010) baySeq: empirical Bayesian methods for identifying differential expression in sequence count data. *BMC Bioinformatics*, **11**, 422.
64. Yin, H., Copley, C.O., Goodrich, L.V. and Deans, M.R. (2012) Comparison of phenotypes between different vangl2 mutants demonstrates dominant effects of the Looptail mutation during hair cell development. *PLoS One*, **7**, e31988.